ELSEVIER

Computational Materials Science 3 (1995) 465–474

COMPUTATIONAL MATERIALS SCIENCE

# An improved model for simulating impedance spectroscopy

R.T. Coverdale [a,*], H.M. Jennings [a], E.J. Garboczi [b]

[a] *Northwestern University, Depts. of Materials Science and Engineering and Civil Engineering Evanston, IL 60208, USA*
[b] *National Institute of Standards and Technology, Building and Fire Research Laboratory, Building Materials Division 226/B348 Gaithersburg, MD 20899, USA*

Received 23 May 1994; accepted 21 August 1994

**Abstract**

A numerical method for simulating the frequency-dependent impedance response of multi-phase composite materials has been developed. The algorithm takes as input 1) a digital image of a microstructure, in two or three dimensions, of any specified composite material, and 2) the frequency-dependent electrical properties of the individual phases of the composite. An impedance spectrum of any frequency range can then be computed using a conjugate gradient algorithm operating on a finite difference solution scheme of Laplace's equation. Examples are given of the impedance of analytically solvable microstructures, to validate the algorithm, and of a random system, to test the usefulness of two different effective medium theories.

## 1. Introduction

Impedance spectroscopy (IS) is a useful, non-destructive tool for analyzing many properties of electroceramic materials [1]. In this technique, a small, single-frequency AC field is applied to a sample, and the amplitude and phase of the resulting current measured. The amplitude of the AC signal is chosen to be small enough to assume a linear response of the material. Usually the impedance, the ratio of the applied voltage to the resulting current, is computed and analyzed.

Recently, IS has been applied to analyze the microstructure of cement paste via its impedance response [2–6]. Most experimental techniques for analyzing pore structure, like scanning electron microscopy or mercury intrusion porosimetry [7], require drying and/or high vacuum. Because the properties and microstructure of cement paste are sensitive to the current moisture state and history of the material, these kind of microstructural analyses are often difficult to interpret, since removal of moisture can significantly change the microstructure. The development of a non-destructive, in situ microstructural analysis technique like IS, therefore, is proving to be useful for studies of the development of microstructure in hydrating cement pastes.

Interpreting the results of IS experiments to give information on microstructure, especially for complex materials like cement-based materials, requires some kind of theoretical model. Most

* Permanent address: Master Builders, Inc., 23700 Chagrin Boulevard, Cleveland, Ohio 44122, USA.


*SSDI* 0927-0256(95)00005-4

experimental results are interpreted in terms of series or parallel combinations of resistors and capacitors and special elements like the "constant phase element" (CPE) [1]. The choice of parameters in these models are not always unique, resulting in some degree of inherent ambiguity. Also, it is often incorrect to describe the complex topology of real microstructures by using simple series and parallel ideas. This has been the reason for using more complicated elements like the CPE element. These elements, however, while they can give reasonable fits to IS data, are not easily related to microstructural features.

The approach taken in this work has been to first represent microstructure via digital image-based models [8–9] or actual 2D micrographs. X-ray tomography can also be used to give experimentally-determined 3D microstructures [10]. Therefore the starting point is an actual or simulated microstructure that is numerically stored and thus can be numerically analyzed. Various physical properties of these 2D or 3D microstructural images can then be computed using exact finite-difference or finite element algorithms. "Exact" means that the correct properties are computed for the given microstructure and choice of individual phase properties, within the limit of the finite resolution of microstructural features in the digital image. In this way the arrangement of phases within the microstructure can be correlated directly with observed bulk properties. An overall review of this modeling approach for cement-based materials has been presented by Garboczi and Bentz [11,12] The approach is readily generalized to other materials [13].

The computational scheme described in this paper is a continuation of previous work on the simulation of IS experiments [14]. The previous work used the Y–$\nabla$ algorithm [15], which is limited to two dimensions but is very efficient. This algorithm directly computes the admittance of a heterogeneous microstructure, without actually solving Laplace's equation for the system. In most cases, however, microstructure must be represented in three dimensions to accurately represent complicated geometries and especially percolation phenomena. The ideas behind the Y–$\nabla$ algorithm [14] have been generalized and extended to develop the three dimensional Fogelholm algorithm [16]. The Fogelholm algorithm becomes extremely slow for systems where the highly conducting phase is far from a percolation threshold [16,17]. Since most materials of interest are not necessarily near to such a percolation thereshold, we have developed a new algorithm, based on a different approach.

This new algorithm uses a finite difference approach and a conjugate gradient algorithm to solve the AC electrical equations. This algorithm is the complex analog of a previous algorithm that solved DC composite electrical problems [8], and may be applied to either two- or three-dimensional images. The method vectorizes well, and so runs very efficiently on modern vector supercomputers. This algorithm allows IS experiments to be simulated on arbitrary three dimensional systems.

## 2. Simulation of impedance spectra

Two basic assumptions implicit in the present algorithm are: 1) the microstructure of interest can be accurately represented as a 2D or 3D digital image, where each pixel of the image is treated as a homogeneous single phase, and 2) the impedance of each individual phase in the composite is known at arbitrary frequencies, either experimentally as a list of numbers, or by using a fitted circuit model to represent the single phase properties. In this paper, we show examples of use of the algorithm on models where a simple RC circuit, consisting of a perfect resistor and perfect capacitor placed in parallel, is used to represent single-phase properties. Because of the random geometry in composite materials, complicated composite IS behavior is commonly encountered, even when the single phase properties are given by simple RC circuits.

Fig. 1 shows a portion of a two dimensional image, in which electrodes are simulated by placing an extra layer of pixels on opposite sides of the image. The resistances ($R$) and capacitances ($C$) for each phase are uniquely determined by that phase's resistivity and dielectric constant, respectively. Different electrical properties may

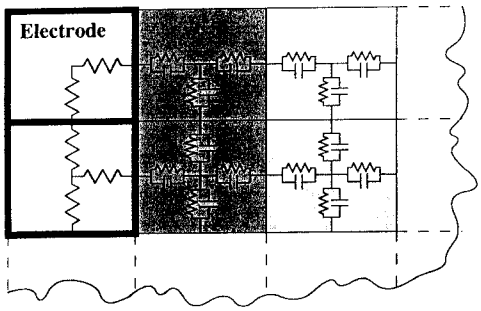


Fig. 1. Part of a 2D image showing how the resistor–capacitor network is mapped onto the digital image of the microstructure.

be assigned to the sample-electrode interface, if necessary, to simulate electrode effects.

The $R$ and $C$ values used in the circuits for each pixel are:

$$R = (\sigma A/D)^{-1}, \tag{1}$$

$$C = k_r \epsilon_o A/D, \tag{2}$$

where $\sigma$ is the conductivity of the specified phase, $k_r = \epsilon/\epsilon_o$ is the dielectric constant, $\epsilon_o$ is the permittivity of free space, $D$ is the length between the center of the pixel and the edge of the pixel (1/2 unit), and $A$ is the area of the pixel face (1 unit$^2$). It is possible to assign a scale to the digital images, e.g. pixel length = 1 mm, but for the purpose of this description each pixel has a length of one unit.

The admittance $\psi$, which is the reciprocal of impedance, is the AC analog of conductance. For each RC circuit at each applied frequency, the admittance is then given by:

$$\psi = 1/R_j + i\omega C_j, \tag{3}$$

where the subscript $(j)$ refers to the $j$th phase of the microstructure, $R$ and $C$ are as defined above, $\omega$ is the applied angular frequency, and $i = \sqrt{-1}$. The sample size is much smaller than the wavelength associated with the applied frequency, so that the same value of $\omega$ is used at each pixel. Each pixel has four (2D) or six (3D) impedances extending from its center to the pixel boundaries (see Fig. 1). Neighboring pixels are connected together by joining the appropriate impedances into a single bond. Perfect bonds are usually assumed between different phases. However, special internal-interface elements could be easily inserted if necessary.

The end result is the creation of a two or three dimensional electrical network with a node at the center of each pixel. The solution of Kirchoff's law on this impedance network is mathematically equivalent to a finite-difference solution of Laplace's equation, $\nabla \cdot j = \nabla^2 V = 0$, where $j = \psi E$, $E = -\nabla V$, and $\psi$ is the admittance [18]. This equation comes from the static (time-independent) limit of the continuity equation [19]. The well-known "correspondence principle" relating static ($\omega = 0$) elastic problems to single-frequency viscoelastic problems [20] has its analogy for electrical problems as well, which we have exploited in developing this algorithm. The mathematics is the same for the single-frequency complex case as for the DC case, but all quantities are allowed to be complex and therefore dependent on frequency.

The impedance calculation begins by applying a voltage across the microstructure, i.e. the field of pixels. This is accomplished, using a unit voltage step, by setting the voltage of the electrode pixel nodes on one side of the image to 1, and those on the opposing side of the image to 0. Since the applied voltage step is taken to have a zero phase angle, the voltage at the electrodes is real and is not a function of frequency. However, the voltages at the pixel-nodes within the sample will be complex, in general, and are iterated until the net current at each node is zero, satisfying Kirchoff's law [19]. Knowing the voltage at each pixel, it is possible to calculate all the local currents, as well as the total current across the sample, and hence, the composite impedance. A similar technique was employed [8] for DC studies of a three-dimensional cement paste model. Since the nodes in this model are connected by impedances instead of only resistors, the network now has a frequency-dependent response.

Periodic boundaries are maintained in directions perpendicular to the applied field by connecting pixels located on a surface of the image to the pixels on the opposite surface. This re-

duces statistical errors associated with using finite-size digital images. If sample-electrode phenomena are not of interest, then periodicity can also be used in the field direction, while still maintaining the applied field [8]. Otherwise, special interface resistors and capacitors can be inserted between the electrode and the sample pixels to mimic the sample-electrode interfacial response.

Solving Kirchoff's law at each of $N$ nodes leads to an independent set of $N$ linear equations that can be arranged into a matrix of the type $\boldsymbol{Ax} = \boldsymbol{b}$, where $\boldsymbol{A}_{ij}$ is the admittance between nodes $i$ and $j$, $\boldsymbol{x}$ is the voltage vector of length $N$, and $\boldsymbol{b}$ is a constant vector, also of length $N$, that comes from the constraints in the system. The constraints in this system are periodic boundary conditions perpendicular to the applied field, and the constant electrode voltages. A matrix equation of this type for the nodal voltages lends itself well to a conjugate gradient iteration technique [21]. The iteration process stops when the magnitude of the maximum residual current going in to a node, averaged over all nodes, is below a prescribed cutoff, chosen low enough to ensure an accurate solution, but not so low that computer time is wasted on achieving more than the necessary accuracy. Since there is one equation and one unknown voltage for each node, a three-dimensional, $100^3$ image, for example, will contain one million equations and unknowns. In general, the matrix A has elements connecting each node to every other node. Fortunately, in a 3D system, only 7 of the $\boldsymbol{A}$ coefficients for each node are non-zero. These 7 elements come from the six connections from each node to its nearest neighbors to a central site, plus a self term.

Memory and computational speed are the limiting constraints on the size of models that can be used. The memory requirements are on the order of 100 bytes per pixel, when all real numbers are double precision (eight bytes per real number). For each applied frequency, a typical $100^3$ system is solved in approximately 1600 seconds on a Cray-YMP supercomputer. Usually, a single spectrum requires at least 20 different frequencies to be sampled. Other versions of the conjugate gradient algorithm may give better performance [22].

## 3. Model verification: exactly solvable test cases

In order to verify the model for random multi-phase composite microstructures, it is necessary to show that the simulation scheme described above is correct by computing the impedance of simpler microstructures for which analytical solutions exist. Four analytically solvable models will be studied numerically.

The first example is the simplest: a single phase material that has a DC conductivity $\sigma = 0.05$ S/unit (mho/unit) and a relative dielectric constant $k_r = 1000$. Fig. 2 shows the Nyquist plot [1] of this system, where the negative of the imaginary part of the impedance is plotted against the real part of the impedance. The solid line is the exact impedance, and the circles are numerical results. The DC resistance of the sample ($R$) is shown to be $0.4\Omega$. Eq. (1) may be used to convert this resistance to conductivity, where $A$ is equal to $50 \times 50 = 2500$ units$^2$, and $D$ is equal to 50 units since the image used is $50^3$ in size. The conductivity for the system is 0.05 S/unit, as expected. The capacitance, and hence $k_r$, is determined by $R$ and $\omega_0$, the angular frequency at the peak of the arc in a Nyquist plot. For a homogeneous system,

$$\omega_o = \frac{\sigma}{k_r \epsilon_o}, \tag{4}$$

where $\sigma$ is the DC conductivity of the system, and $k_r$ and $\epsilon_o$ are as defined before. Since we can establish both $\sigma$ and $\omega_o$ from the impedance curve, $k_r$ can be calculated directly. Approximately locating the arc maximum by interpolating between the data points displayed in Fig. 2 gives a value of $k_r = 1036$, an error of only 3.6%. This error can be attributed to approximating the position of the arc peak, and thus the value of $\omega_o$. In this case, since we knew $\omega_o$ analytically, the value of $k_r$ could have been computed even more accurately. However, the interpolation method would be that used in a simulation of a general microstructure, where no analytical results would be available. Table 1 shows the absolute magnitude of impedance, $|Z|$, for several different frequencies, showing the accuracy available when the frequency is precisely known. The relative errors

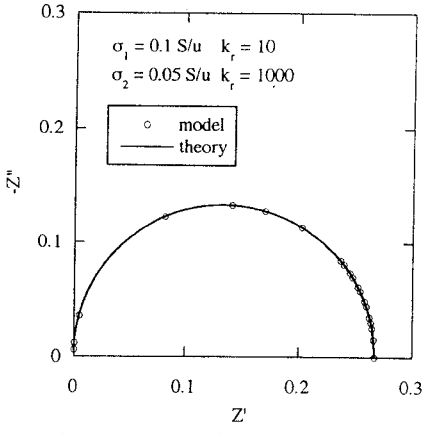


Fig. 2. Nyquist plot for a single phase material, whose admittance is given at all frequencies by $\psi = \sigma + ik_r\omega$, $\sigma = 0.05$ S/unit, $k_r = 1000$.

shown in column 5 are due to computer round off only.

The next two cases considered are two phase composites, with each phase occupying half the volume, arranged in series or parallel, as shown in Fig. 3. The DC composite conductivity for each of these cases is [23]:

$$\text{(Series)}\ \sigma = (c_1/\sigma_1 + c_2/\sigma_2)^{-1}, \tag{5}$$

$$\text{(Parallel)}\ \sigma = c_1\sigma_1 + c_2\sigma_2, \tag{6}$$

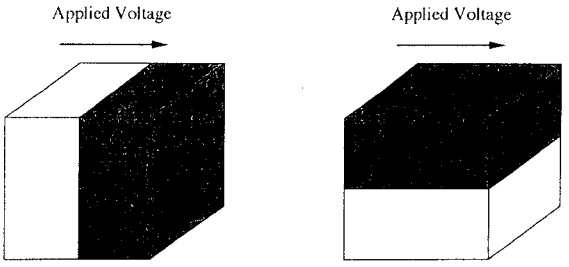


Fig. 3. 2D cross sections of a series and parallel arrangement of the phases in a two-phase composite.

where $\sigma$ is the conductivity of the composite microstructure, and $\sigma_1$, $c_1$, $\sigma_2$, and $c_2$ are the DC conductivity and volume fraction of phases 1 and 2, respectively. The same equations apply if the admittance $\psi$ is substituted for conductivity.

The calculated impedance curve for the series microstructure is shown in Fig. 4 along with values determined from a $50^3$ image. Fig. 5 shows a similar plot for the parallel arrangement. In each case, the model has accurately determined the impedance curve. Numerical comparisons of $|Z|$ at different frequencies for both the series and parallel case are also shown in Table 1.

The last example is somewhat more complicated and consists of a dilute distribution of insu-

Table 1
Comparison of computational and analytical results for the absolute value of the impedance of the single phase, series, parallel, and dilute sphere suspension examples. The applied frequency is $f$, and $|Z| = [(\text{Re } Z)^2 + )\text{Im } Z)^2]^{1/2}$ is the absolute value of the impedance.

| System | $f$ | $\|Z\|$ model | $\|Z\|$ theory | % error |
|---|---|---|---|---|
| single phase | 0 Hz | 0.40000 | 0.40000 | 0 |
| | 500 KHz | 0.28129 | 0.28270 | 0.279 |
| | 60 MHz | 0.08726 | 0.08772 | 0.529 |
| series | 0 Hz | 0.30000 | 0.30000 | 0 |
| | 90 KHz | 0.22324 | 0.22375 | 0.228 |
| | 200 MHz | 0.06733 | 0.06754 | 0.311 |
| parallel | 0 Hz | 0.26667 | 0.26667 | 0 |
| | 900 KHz | 0.26206 | 0.26211 | 0.019 |
| | 4 MHz | 0.01179 | 0.01185 | 0.506 |
| sphere | 0 Hz | 0.10115 | 0.10115 | 0 |
| | 6.07 MHz | 0.09688 | 0.09678 | 0.103 |
| | 1.76 GHz | 0.06792 | 0.06768 | 0.351 |

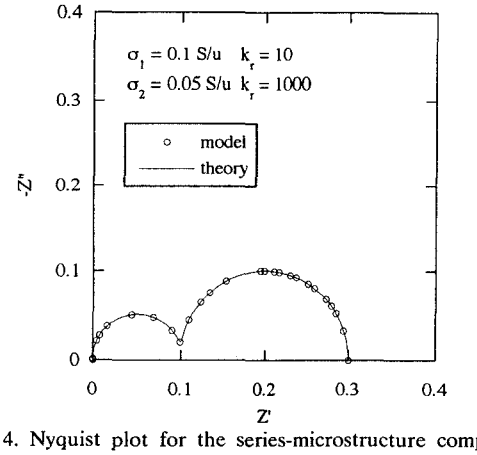


Fig. 4. Nyquist plot for the series-microstructure composite material, where the admittances of the two phases is as shown in the figure.

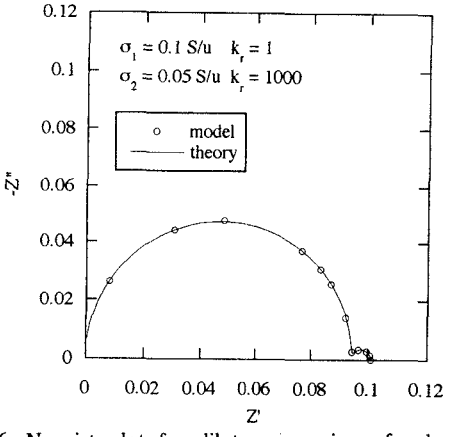


Fig. 6. Nyquist plot for dilute suspension of spheres microstructure, where the admittances of the two phases are given in the figure. Phase 1 is the matrix, phase 2 is the spherical inclusions.

lating spheres in a conducting cube. "Dilute" means that the volume fraction of the spheres is small enough so that each sphere does not interact with the other spheres. In this case, the DC conductivity of the composite is [24]:

$$\sigma = \sigma_1 + 3c_2(\sigma_2 - \sigma_1)/(2\sigma_1 + \sigma_2), \qquad (7)$$

where the terms have the same meanings as before, and the insulating sphere is phase 2. This equation may also be converted to admittance to provide an analytical solution for the impedance spectra. The electrical parameters for the example considered are $\sigma_1 = 0.1$, $\sigma_2 = 0.05$, $k_1 = 1$, $k_2 = 1000$. Both the analytical solution and model results are shown in Fig. 6, and are in good agreement. The sphere is simulated by a digital representation that has a diameter of 33 pixels, and is placed in the center of a $100^3$ cube, having periodic boundary conditions. The sphere has a volume fraction of 0.018. A single sphere can be simulated to give the correct result for a dilute concentration of spheres, since Eq. (7) is based on the assumption of non-interacting spheres. It is known that the admittance of a periodic array of spheres, which result from the periodic boundary conditions used, is the same as Eq. (7) up to the linear order term in the sphere volume fraction [25]. Some error is also incurred because the insulating sphere in the model is only a digital representation of a true continuum sphere. Nevertheless, the model has accurately described the complex electrical behavior for this system, as can be seen in Table 1 and Fig. 6.

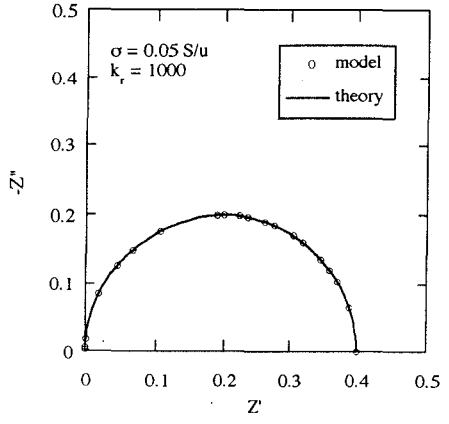


Fig. 5. Nyquist plot for the parallel-microstructure composite material, where the admittances of the two phases is as shown in the figure.

It is interesting to note that Fig. 6 clearly displays two arcs. In fact, it has been shown that the analytical solution in Eq. (7) can be mapped exactly onto two RC parallel circuits arranged in series [26]. Two-arc behavior like this is often taken to mean that a series arrangement of the phases exists (see Fig. 4), since a parallel arrangement of phases will only show one arc (see Fig.

5). However, it is physically not possible to consider the dilute sphere suspension microstructure as either a parallel or a series arrangement of phases. Rather, since the current must flow around and through the spheres, there is a degree of tortuosity present, which gives a more complicated response. This behavior will be present for any choice of the individual phase admittance parameters, although two arcs will only be visually observed when there is a significant difference between the two resonant frequencies, $\omega_1 = \sigma_1/k_1$ and $\omega_2 = \sigma_2/k_2$. In Bonanos' exact mapping to two RC parallel circuits in series [26], the resistors and capacitors defined by Eq. (7) contain terms relating to the individual phase admittances and phase fractions of both phases, so the two "phases" that appear to be in series are actually some mathematical combination of the two actual phases.

Fricke [27] computed the admittance of a dilute suspension of triaxial ($a \neq b \neq c$) ellipsoids, randomly oriented, where matrix and inclusions had arbitrary admittances. He found that for this low concentration limit, the impedance could be expressed as a series combination of four RC circuits. The number four comes from the matrix phase plus one each for the three possible orientations of the ellipsoidal inclusions. These four circuits collapse to three for ellipsoids of revolution ($b = c$), and to two for spheres ($a = b = c$). Therefore inclusion *geometry* also contributes to determining how many arcs will appear in the impedance spectrum, and not just a material's series/parallel character, which usually cannot be defined for a complex microstructure.

One could speculate that two (or more) arc behavior will only be observed if at least one of the phases is discontinuous, as was the case in the above dilute suspensions of inclusions. The next section gives an example of how this hypothesis is not true, in general.

## 4. Two-Phase interpenetrating random network

The final system to be considered is a two phase, interpenetrating composite [28,29] in which both phases are percolated in three dimensions.

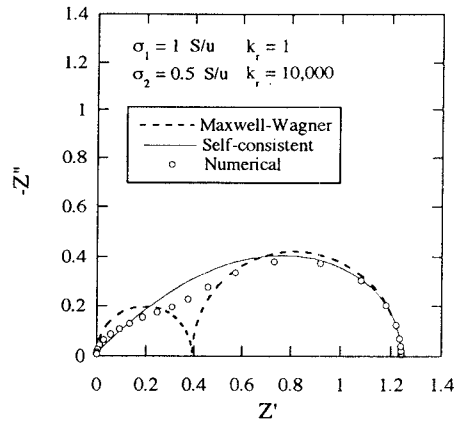


Fig. 7. Nyquist plot for interpenetrating phase composite model of overlapping spheres. Phase 1 is the matrix, phase 2 is the phase made up from the overlapping spheres. The volume fraction of phase 2 is 0.34.

The phases have the following properties: $\sigma_1 = 1.0$, $\sigma_2 = 0.5$, $k_1 = 1$, $k_2 = 10\,000$. Phase 2 is formed by placing overlapping spheres at random locations in the digital microstructure. Periodic boundary conditions were maintained during the sphere placement process. Each sphere had a diameter of 9 pixels, and was placed in a $64^3$ unit cell, giving volume fractions $c_1 = 0.66$ and $c_2 = 0.34$.

The Nyquist plot of the impedance curve of this system is shown in Fig. 7. The data points clearly show that there is more than one arc present, and most probably many arcs, with a distribution of resonant frequencies. However, using a burning algorithm on the digital image [30,31] model, both phases were found to be fully percolated and continuous. The dashed line in Fig. 7 is the Maxwell–Wagner Eq. [1], an effective medium theory equation based on spherical inclusions:

$$\psi = \psi_1 = \frac{[2\psi_1 + \psi_2 - 2x_2(\psi_1 - \psi_2)]}{[2\psi_1 + \psi_2 + x_2(\psi_1 - \psi_2)]}, \qquad (8)$$

where $x_2$ is the volume fraction of phase 2, the phase fraction of phase 1 is $1 - x_2$, and $\psi_1$ and $\psi_2$ are the admittances of phases 1 and 2, respectively. The Maxwell–Wagner equation has been shown, like Eq. (7), to be analytically equivalent

to a series combination of two RC (resistor in parallel with a capacitor) circuits [26], which will always show two arc behavior if there is a significant difference in relaxation times between the two arcs. The solid line in Fig. 7 clearly shows two well-separated arcs, which does not agree well with the numerical data points. However, the DC resistivity does matches the numerical result within a few percent.

The Maxwell–Wagner equation does not work well for the overall impedance curve in this case because it cannot take into account the overlapping of the spheres which eventually leads to the percolation of the sphere phase. Eq. (8) does not have a percolation threshold. This is easily proven by letting $\psi_2$ go to $\infty$, which does not produce an infinite value of $\psi$ for any value of $x_2 < 1$. However, letting $\psi_1$ go to zero results in $\psi$ being zero for any value of $x_2$. This result means that in the Maxwell–Wagner "microstructure" implied by the equation's derivation, phase 1 is always percolated and phase 2 is never percolated.

The dashed line in Fig. 7 is a variation of Eq. (8), often referred to as the "self-consistent" approach [32]. This theoretical value for the impedance matches the overall curve much more closely than did the Maxwell–Wagner equation. It is obtained by modifying the derivation of Eq. (8) by letting the embedding medium in the derivation be the effective medium, rather than the pure matrix phase [32]. This treats phases 1 and 2 on an equal basis, thereby eliminating the distinction between "matrix" and "inclusion". The resulting prediction for the effective conductivity is:

$$\psi = \tfrac{1}{4}\Big[-(3x_2-2)\psi_1 - (1-3x_2)\psi_2 + \Big\{\big[(3x_2-2)\psi_1 + (1-3_2)\psi_2\big]^2 + 8\psi_1\psi_2\Big\}^{1/2}\Big], \quad (9)$$

where the parameters are the same as in Eq. (8), and the square root is the complex square root. Eq. (9) is the solution to the quadratic equation that results from making Eq. (8) self-consistent. Eq. (9) does display a percolation threshold. In the limit where $\psi_2$ approaches zero, Eq. (9) gives a critical value of $x_2$ of 1/3. The actual critical value of $x_2$ for overlapping spheres to percolate is $x_2 = 0.29$ [33]. This is why Eq. (9) matches the overall shape of the impedance curve better than did Eq. (8). Although we have not checked this explicitly, it is almost certain that Eq. (9) is not expressible as a finite number of RC circuits, but rather produces a continuous spectrum of resonant frequencies. The overlapping sphere microstructure, like many real random microstructures, has many differently-shaped microstructural features, and thus shows a broadened, non-circular Nyquist impedance plot.

## 5. Discussion and conclusions

A computer algorithm has been developed that can accurately compute the impedance spectrum of a simulated microstructure in two or three dimensions. Model inputs include: 1) a digital representation of microstructure and 2) the electrical properties of each individual phase of the microstructure. The individual phase electrical properties can be read from a table of experimentally known values or can be simulated using a fitted circuit.

The calculation scheme has been shown to be very accurate for composite systems with known solutions, which provides a basis for extending the model to more complicated multi-phase composites whose solution are not known analytically.

The overlapping sphere, interpenetrating phase composite model demonstrated how non-circular, multiple arc behavior can appear even when both phases of a random two-phase composite are fully percolated. Thus what is usually referred to as "series-like behavior" can result even when it is not possible to characterize the microstructure as being a series combination of phases in any way. Also, the dangers in inferring microstructure from DC characteristics alone were clearly seen in Fig. 7, which showed that both the Maxwell–Wagner and self-consistent effective medium theories gave accurate (within a few percent) predictions of the DC resistivity. The percolation aspects of the microstructures implied by these two equations are much different, however. The addi-

tional use of finite frequency data showed that the self-consistent theory gave a reasonably good prediction for the overall character of the impedance curve, while the Maxwell–Wagner equation badly misrepresented the shape of the impedance curve.

While this approach has been developed to study the impedance response of cement-based materials, it is generally applicable to any heterogeneous material whose microstructure can be represented by a two- or three-dimensional digital image, if the electrical properties of the individual phases of the microstructure are known. Perfect bonding between phases is usually assumed, although interface impedances can be readily handled by the algorithm. A direct digital image representation of microstructure that can be compared with accurate numerical impedances allows quantitative microstructure-property relationships to be developed.

The ability to directly compute the impedance curve of any microstructure allows better microstructural inferences from experimental IS curves, removing dependence on overly simple resistor–capacitor circuit models. Such circuit models are often very useful, and even quantitatively accurate in some instances, but will only hinder progress in using IS in the study of the complex microstructure of random composite materials [34,35].

Current computing capabilities of machines that are generally available to the average academic user limit three-dimensional models to sizes not much larger than $100^3$, although that limit will only improve as larger memory and higher speed computers become more widely available to the materials science community. These improvements in computing power will make possible the use of higher resolution digital images, which will in turn result in more accurate numerical predictions of the complex electrical properties of materials with intricate random microstructures.

## Acknowledgements

The authors would like to acknowledge the National Science Foundation's Center for Science and Technology for Advanced Cement Based Materials, under grant number DMR-08432, for financial support. Supercomputing facilities were provided by the National Center for Super Computing Applications at the University of Illinois at Champaign-Urbana, under grant number DMR-920024N.

## References

[1] J.R. MacDonald and W.B. Johnson, Fundamentals of Impedance Spectroscopy, in: Impedance Spectroscopy: Emphasizing Solid Materials and Systems, eds. J.R. MacDonald. (Wiley, New York, 1987) pp. 12–26.
[2] C.A. Scuderi, T.O. Mason and H.M. Jennings, J. Mat. Sci. Lett. 7 (1988) 1056.
[3] B.J. Christensen, T.O. Mason and H.M. Jennings, J. Am. Ceram. Soc. 75 (1992) 939.
[4] Z. Xu, P. Gu, P. Xie and J.J. Beaudoin, Cem. Conc. Res., in press.
[5] P. Gu, P. Xie, J.J. Beaudoin and R. Brouseau, Cem. Concr. Res. 22 (1992) 833.
[6] P. Xie, P. Gu, Z. Xu and J.J. Beaudoin, Cem. Concr. Res. 23 (1993) 359.
[7] H.F.W. Taylor, Cement Chemistry (Academic Press, London, 1990).
[8] E.J. Garboczi and D.P. Bentz, J. Mat. Sci. 27 (1992) 2083.
[9] E.J. Garboczi and D.P. Bentz, J. Mat. Res. 6 (1991) 196.
[10] L.M. Schwartz, F. Auzerais, J. Dunsmuir, N. Martys, D.P. Bentz and S. Torquato, to be published in Physica A: Proc. 3rd Int. Meeting on Electrical Transport and Optical Properties of Inhomogeneous Materials (ETOPIM3), Guanajuato, Mexico, 9–13 August 1993.
[11] E.J. Garboczi and D.P.Bentz, Fundamental Computer Simulation Models for Cement-Based Materials, in: Materials Science of Concrete. Vol. 2, ed. J. Skalny (Am. Ceram. Soc., Westerville, Ohio, 1991).
[12] E.J. Garboczi and D.P. Bentz, Mater. Res. Soc. Bulletin 18, 50–54 (1993) 50.
[13] P.J.Q. Pimienta, E.J. Garboczi and W.C. Carter, Comput. Mater. Sci. *1* (1992) 63.
[14] R.T. Coverdale, E.J. Garboczi, B.J. Christensen, T.O. Mason and H.M. Jennings, J. Am. Ceram. Soc. 76 (1993) 1153.
[15] D.J. Frank and C.J. Lobb, Phys. Rev. B 37 (1988) 302.
[16] D.B. Gingold and C.J. Lobb, Phys. Rev. B 42 (1990) 8220.
[17] D.P. Bentz, E.J. Garboczi, D.B. Gingold, C.J. Lobb and H.M. Jennings, Ceram. Trans. 16 (1990) 227.
[18] S Kirkpatrick, Rev. Mod. Phys. 45 (1973) 574.
[19] J.R. Reitz and F.J. Milford, Theory, 2nd Edition (Addison-Wesley, Reading MA, 1967).
[20] R.M. Christensen, Theory of Viscoelasticity: An Introduction (Academic Press, New York, 1982).

[21] W.H. Press, B.P. Flannery, S.A. Teukolsky and W.T. Vetterling, Numerical Recipes: The Art of Scientific Computing (FORTRAN Version) (Cambridge University Press, Cambridge, 1989).
[22] A.R. Day and E.J. Garboczi, unpublished.
[23] Z. Hashin, J. Appl. Mech. 50 (1983) 481.
[24] Ref. [1], small $x_2$ limit of Eq. (14), p. 198.
[25] A.S. Sangani and A. Acrivos, Proc. R. Soc. Lond. A 386 (1982) 263.
[26] N. Bonanos and E. Lilley, J. Phys. Chem. Solids 42 (1981) 943.
[27] H. Fricke, J. Phys. Chem. 57 (1953) 934.
[28] D.R. Clarke, J. Amer. Ceram. Soc. 75 (1992) 739.
[29] D.S. McLachlan, M.B. Blaszkiewicz and R.E. Newnham, J. Am. Ceram. Soc. 73 (8) (1990) 2187.
[30] D. Stauffer, Introduction to Percolation Theory (Taylor and Francis, London, 1985).
[31] D.P. Bentz and E.J. Garboczi, Cem. Conc. Res. 21 (1991) 325.
[32] R. Landauer, AIP Conf. Proc. No. 40, Electrical Transport and Optical Properties of Inhomogeneous Media. Eds. J.C. Garland and D.B. Tanner (Am. Inst. Phys., New York, 1978) pp. 2–45.
[33] E.J. Garboczi, M.F. Thorpe, M. DeVries and A.R. Day, Phys. Rev. A43 (1991) 6473.
[34] R.T. Coverdale, B.J. Christensen, H.M. Jennings, T.O. Mason, D.P. Bentz and E.J. Garboczi, J. Mater. Sci. 30 (1995) 712.
[35] R.T. Coverdale, B.J. Christensen, T.O. Mason, H.M. Jennings and E.J. Garboczi, J. Mater. Sci. 29 (1994) 4984.